Heterogeneity in the Actions of Drugs That Bind in the DNA Minor Groove†

Fred G. Albert, Todd T. Eckdahl,‡ Daniel J. Fitzgerald, and John N. Anderson*

Department of Biological Sciences, Purdue University, West Lafayette, Indiana 47907-1392

Received February 16, 1999; Revised Manuscript Received May 25, 1999

ABSTRACT: Distamycin and Hoechst 33258 have long served as the model compounds for biochemical, biophysical, and clinical studies of the drugs that bind in the DNA minor groove. However, the results presented in this investigation clearly show that 4,6-diamidino-2 phenylindole (DAPI) is superior to both of these drugs at negating the effects of intrinsic DNA curvature and anisotropic bendability as measured by electrophoretic and ligation analysis. In addition, DAPI was more effective than distamycin and Hoechst 33258 at inhibiting the assembly of nucleosomes onto synthetic and natural sequences that have multiple closely spaced oligo-AT sequences that serve as drug binding sites. Since these effects may be related to the biological action of the drugs, it was of interest to determine the mechanism that was responsible for the enhanced action of DAPI. The possibility that the differential drug potencies resulted from differential overall affinities of the ligands for A-tract molecules was considered, but drug binding studies suggested that this was not the case. It is also unlikely that the differential drug effects resulted from the binding of the drugs to different DNA sites since the oligo A/T binding sites for DAPI and Hoechst were centered on the same nucleotide positions as revealed by footprinting studies using exonuclease III, DNase I, and hydroxyl radical. However, the footprinting studies with DNase I did uncover a potentially important difference between the drugs. DAPI protected only the AT bp in the binding sites, while distamycin and Hoechst protected these bp as well as flanking Gs and Cs. These results permitted us to advance a preliminary model for the enhanced action DAPI. According to the model, the short length of DAPI and its absolute specificity for A/T bps with narrow minor grooves ensures that only particularly minor grooves that give rise to curvature and anisotropic bendability are occupied by the drug. Consequently, each helical deflection induced by an A-tract in the absence of the drug is countered by an opposite deflection induced by DAPI binding, thus effectively neutralizing intrinsic curvature and bending into the minor groove.

Drugs that bind in the minor groove of DNA have attracted much interest because of their diverse antimicrobial and antitumor activities (reviewed in refs *1*−*3*). These minor groove binding drugs (MGBD)[1] have also served as model compounds for studies of proteins that bind in the DNA minor groove including HMG box transcription factors and the TATA box binding protein (*4*, *5*). Well-known examples of this class of compounds include the antibiotic distamycin A and the fluorochromes Hoechst 33258 and 4,6-diamidino-2 phenylindole (DAPI). These compounds are particularly well suited for comparative studies on natural DNA and DNA in the chromosome since crystal structures of their complexes with oligonucleotides have been published (*2*, *6*−*14*) which are complemented by numerous solution studies of the drugs bound to DNA (*1*, *15*−*32*). Both approaches have revealed that the ligands interact preferentially with AT-rich sequences that are at least 3−4 bp in length. The preference of these drugs for AT sites has been attributed to the narrow minor groove that characterizes these sequences and to the complementary crescent shape of most of these ligands which fits snugly edgewise into the groove. Strong van der Waals contacts between the sides of the groove and the aromatic rings of the bound drug provide a significant contribution to the stability of the ligand−DNA complex. The stability of the bound cationic drugs is further enhanced by interactions between the negative electrostatic potential of the AT sequences and by hydrogen bonding between the ligand and DNA which replaces the ordered spine of hydration. The relative importance of these factors for the stability of the DNA−drug complex remains a matter of discussion and is likely that their contributions vary in a drug- and DNA-dependent manner (*1*, *2*).

The biological effects of the MGBD are presumably due to their inhibitory effects on transcription and replication (reviewed in ref *1* and *3*). However, the precise genomic targets and modes of action of these ligands are not known. Most studies have focused on the abilities of the MGBD to inhibit the binding of regulatory proteins to oligonucleotide-length recognition sequences that are rich in A and T base pairs. For example, these drugs have been reported to inhibit the DNA binding of certain restriction enzymes, the TATA box binding protein, the antennapedia homeodomain protein, the ubiquitous octamer binding protein, and the erythroid-specific GATAAG protein (*1*, *33*−*40*). Thus, there has been

† This work was supported in part by the Walther Cancer Foundation.

* To whom correspondence should be addressed. Tel: 765-494-4998. Fax: 765-494-0876.

‡ Present address: Department of Biology, Missouri Western State College, 4325 Downs Drive, St. Joseph, MO 64507.

[1] Abbreviations: MGBD, minor groove binding drugs; DAPI, 4,6-diamidino-2-phenylindole; Hoechst, Hoechst 33258; ExoIII, exonuclease III; $OH^{\bullet}$, hydroxyl radical; PCR, polymerase chain reaction; PA, polyacrylamide; bp, base pair; ARS, autonomous replicating sequence.

10.1021/bi990382p CCC: $18.00
Published on Web 07/14/1999

a tremendous effort expended during the past decade toward the development of MGBD analogues that display enhanced DNA binding specificities in the hope of targeting the ligands to specific oligonucleotide-length sites in the genome.

Our recent studies have uncovered a novel specificity of the MGBD that requires long segments (≥120 bp) of A + T-rich DNA (*41*). In these studies, it was shown that DAPI selectively inhibited the assembly of intrinsically curved DNA segments into nucleosomes. The marked template specificity for this effect was attributed to ligand binding to multiple closely spaced oligo A/T tracts that give rise to DNA curvature. This inhibitory action is likely to be of biological importance in the action of these drugs since curved DNA segments and other long blocks of oligo A/T-rich DNAs are rare in the genome and are frequently found in control regions for transcription, replication, and recombination (*42*−*46*).

In the present report, we have taken a comparative approach to examine the abilities of three MGBD to selectively inhibit the assembly of nucleosomes onto natural and synthetic DNAs with varying sequence properties and intrinsic structures. These studies were undertaken to further define the features of the DNA template that are required for the actions of these compounds. The effects of the drugs on the nucleosome were then related to their effects on the global curvature of DNA and its anisotropic bendability. We then attempted to explain drug-dependent variations that were seen in the results of these experiments by characterizing the DNA binding sites for the ligands. The results indicate that certain actions of the drugs on nucleosomal and naked DNA can readily be explained by variations in binding sites while other effects seem to depend on postbinding features of the DNA−ligand complexes.

MATERIALS AND METHODS

DNA Preparation. The preparation of most of the natural DNA fragments and synthetic sequences used in this study has been described previously (*41*, *42*, *44*, *46*, *47*). Labeled DNA for ligation and electrophoretic studies was prepared by standard end-labeling with [γ-^{32}p] ATP. The synthetic duplex oligonucleotides used in Figures 2 and 4 were end labeled prior to ligation. Radioactive DNA for footprinting experiments was prepared by the PCR using top strand or bottom strand labeled primers that are centered at 19 bp upstream and 33 bp downstream from the *Eco*RI site and *Hind*III site in pUC18, respectively (see Figure 9). DNA fragments were purified by electrophoresis through agarose gels and appropriate bands eluted from the gels by the crush-soak method. Electrophoretic analysis for DNA bending was carried out as described previously using 6−10% polyacrylamide (PA) gels run in Tris−acetate EDTA (TAE) buffer at 4 °C (*42*). The DNAs at either 1 μg/mL (Figure 4) or 100 μg/mL (Figure 5) were incubated with the indicated concentrations of drugs prior to electrophoresis.

Nucleosome Reconstitutions. Nucleosome reconstitution was carried out by the histone exchange method as described previously (*41*, *47*). Briefly, labeled DNA fragments (∼1 μg/mL) were incubated with H1 stripped chicken erythrocytes oligonucleosomes (∼50 μg/mL) in 20 mM Tris-Cl (pH 8.0) containing 1 M NaCl, 0.1% NP40, and the indicated concentrations of the MGBD. The mixtures were incubated at room temperature for 30 min, and the salt concentration was then lowered to 100 mM by 8−10 additions of 10 mM Tris-Cl (pH 8.0) that were made approximately 20 min apart. Aliquots of the completed reconstitution were run on 5% (70:1) PA gels containing 20% glycerol and 0.5× TBE. In the absence of MGBD, >95% the of label displayed the mobility expected of mononucleosomes. Selected mononucleosome samples also yielded protected fragments of 140−150 bp following digestion by micrococcal nuclease (data not shown).

DNA Binding Analysis. DNA binding drugs were purchased from Sigma. Drug solutions were either freshly prepared in 10 mM Tris-HCl (pH 7.5) containing 10 mM NaCl or stored in the dark in this solution at −20 °C. Stored samples retained full activity when tested as in Figures 3, 5, and 7. The relative binding affinities of DAPI and Hoechst for the curved intron DNA were determined by fluorescence enhancement at 465 nM (*48*). DNA (1 μg/mL) was incubated in 30 mM Tris (pH7.8), 10 mM $MgCl_2$, and 0−10 μM drug. In Figure 8, the analysis was carried out with varying concentrations of synthetic DNA and a fixed (0.2 μM) concentration of drug. In the analysis described in the legend to Figure 8, the DNAs (10 ng/mL) were incubated with varying concentrations (8−1000 nM) of drug. After 30 min of incubation, the samples were diluted to a final volume of 1 mL and the fluorescence was immediately measured. Increasing to 2 h the time between dilution and measurements gave essentially the same values.

Ligation Reactions. Labeled *Eco*RI intron fragment (1.0 μg/mL) mixed with nonradioactive *Eco*RI-digested recombinant plasmid containing the fragment (350 μg/mL) were equilibrated at 5 °C in 30 mM Tris (pH 7.8), 10 mM $MgCl_2$, 10 mM dithiothreitol, and 1 mM ATP in the presence of the indicated concentrations of drugs. These high DNA concentrations favor multimerization of noncircular fragments (*46*, *49*). For the experiment in Figure 7, ligations were initiated by the addition of T4 DNA ligase to a final concentration of 5 U/mL. Samples were removed at the indicated times and added to stop buffer (66 mM EDTA, 5% glycerol, 0.05% bromophenol blue) in order to quench the reaction. One ligated sample set was treated with exonuclease III (ExoIII; 100 U/mL) for 1 h at 37 °C prior to its addition to stop buffer. Ligated products were resolved on 2% agarose gels in TAE containing 1 μg/mL ethidium bromide (*46*). Gels were subsequently dried and autoradiographed. For studies in Figure 6, the ligation reaction was initiated by the addition of T4 ligase at a final concentration of 0.3 U/mL. Aliquots were removed at the indicated time points and treated with ExoIII as described above. The ExoIII-resistant closed circle DNA was fixed to GF/C filters with 5% trichloroacetic acid and 20 mM sodium pyrophosphate. The filters were washed in 70% ethanol and air-dried, and the radioactivity was measured in a standard scintillant.

Inhibition of Restriction Enzyme Activity. In the standard reactions, phage lambda DNA (100 μg/mL) or lambda DNA mixed with radioactive synthetic or intron DNAs was incubated with 0−25 μM MGBD for 20 min prior to digestion by the indicated enzymes. Digestions were for 1 h at 37 °C in standard buffers using 2 U of enzyme/μg of DNA. The extents of inhibition were dependent on DNA concentration, enzyme concentration, and digestion time (data not shown). However, the relative extents of inhibition induced

Table 1: Restriction Enzyme Inhibition by MGBD

enzyme	site	DNA	order of inhibition[a]
Eco RI	GAATTC	lambda	H (5) > Da (10) > Ds (20)
		intron segment	H (5) > Da (10) > Ds (15)
		$(CGGGAATTCC)_{17-23}$	H (5) > Da (10) > Ds (25)
Apo I	AAATTT	intron segment	H (5) > Da (10) = Ds (10)
Eco R5	GATATC	lambda	Ds > H > Da
		$(CGGGATATCC)_{17-23}$	Ds > H > Da
Nde I	CATATG	lambda	H (20) > Da = Ds
Hpa I	GTTAAC	lambda	Ds (15) > H > Da
		$(CGGGTTAACC)_{17-23}$	Ds (15) = H (15) > Da
Dra I	TTTAAA	lambda	Ds (20) = H (20) > Da (25)
Ssp I	AATAAT	lambda	H (5) > Ds (10) = Da (10)
Bam HI	GGATCC	lambda	NI
Pvu II	CAGCTG	lambda	NI
Stu I	AGGCCT	lambda	NI
Hind III	AAGCTT	lambda	NI[b]
Cla I	ATCGAT	lambda	NI[b]

[a] Determined as described in Figure 13. The numbers in parentheses are the μM concentrations of MGBD that give 50% inhibition of the average site. No number indicates that the concentration was >25 μM. NI = Inhibition not observed for any site. [b] A minority of sites which contain flanking A/T bp are inhibited by the MGBD as described in Materials and Methods.

by the MGBD under all conditions were the same as those shown in Table 1. Extents of inhibition were also related to the A + T content of the 4 bp on each side of the enzyme recognition site which has been noted previously (*1*, *36*). For example, the drug sensitivities of the 5 *Eco* R1 sites in lambda DNA analyzed in Figure 12 (top panel) followed the order site 2 > 3 > 5 > 4 > 1 which was correlated with the A + T content of the 4 bp on each side of the recognition site(% A + T = 88, 75, 75, 38, and 25, respectively). This effect was also seen with other enzymes listed in Table 1 and was particularly striking with *Hind* III and *Cla* I that have A or T at the terminal but not central positions in their recognition sites. With these enzymes, only those sites that are flanked by at least 2 bp of A and/or T are protected from enzyme digestion by the MGBD (data not shown).

Footprinting Analysis. A mixture of end-labeled DNA (20 000−50 000 cpm) and nonradioactive phage lambda DNA (100 μg/mL) in 10−30 μL was preincubated at room temperature for 20 min with drugs in 100 mM NaCl, 5 mM $MgCl_2$, and 10 mM Tris-HCl (pH 8.0) prior to digestion. ExoIII digestions were carried out at room temperature for the indicated times using 100 U/mL. DNase I digestions of drug−DNA complexes were carried out for 3 min using 8 U/mL. Reactions were stopped by the addition of an equal volume of formamide dye mixture, and the DNA fragments were then electrophoresed on 8% PA gels in 7.5 M urea. The hydroxyl radical cutting reaction was carried out as described by Burkhoff and Tullius (*50*) for 5 min at room temperature. Digestions were stopped by the addition of thiourea and EDTA, and the DNA was then ethanol precipitated prior to standard sequencing gel analysis.

RESULTS

Nucleosome Assembly. We have previously reported that DAPI selectively inhibited the assembly of a nucleosome onto a highly curved DNA fragment from an intron of the *C. elegans* RNA polymerase gene (*41*). The effect was dependent on the binding of the ligand to the multiple closely spaced oligo A/T tracts that spanned the length of the fragment. However, it was not known if intrinsic curvature per se was also required for the action of the drug nor was it known whether other MGBD display the activity. Since

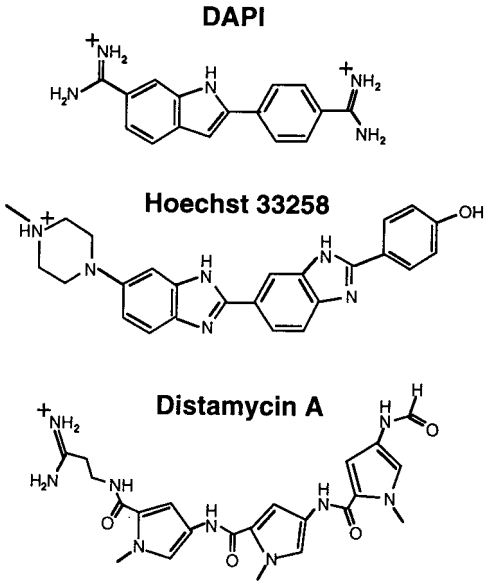

FIGURE 1: Structures of the drugs used in this study.

the inhibition of DNA packaging by the MGBD may be important in their mode of action, we addressed these questions by studying the abilities of the three MGBD shown in Figure 1 to inhibit nucleosome formation on synthetic and natural DNA molecules with different sequence patterns and intrinsic structures.

The sequence pattern of the synthetic duplex DNA molecules used in the studies presented in Figure 2 is of the form $(CGGGN_4CC)_{17-23}$ where N_4 = AAAA, ACAA, AATT, TTAA, or ATAT. As will be shown below, the fragments with the AAAA and AATT motifs display retarded electrophoretic mobilities on PA gels which is indicative of DNA curvature while the other three fragments migrate according to their lengths. In the analysis shown in Figure 2., these DNAs were incubated with nucleosome core particles in 1 M NaCl in the presence of the indicated concentrations of the MGBD. The NaCl concentration was then reduced to 0.1 M by stepwise dilution, and the fraction of the templates that had assembled into mononucleosomes was determined by electrophoresis on PA−glycerol gels. The drugs inhibited the assembly of nucleosomes onto the two

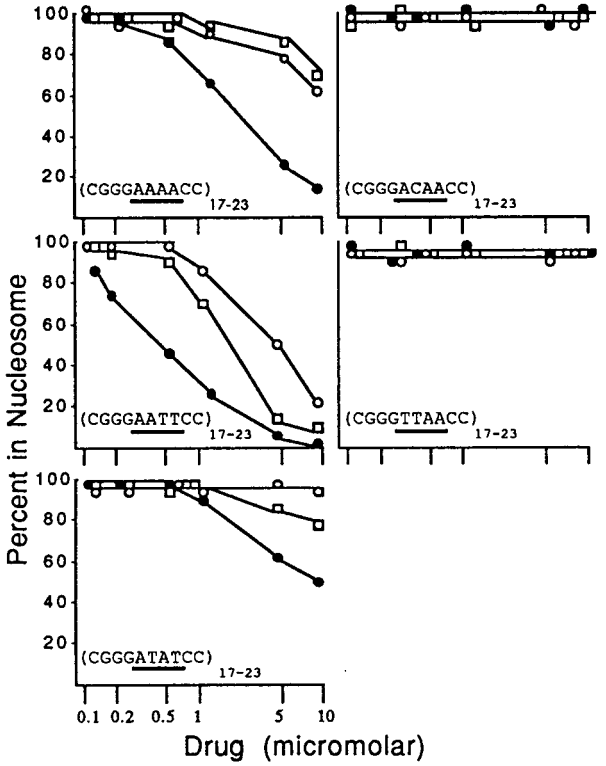

FIGURE 2: Effects of MGBD on the assembly of synthetic DNA into nucleosomes. The indicated synthetic DNA duplex sequences were incubated with various concentrations of DAPI (●), distamycin (○), or Hoechst (□) in 1 M NaCl in the presence of erythrocyte nucleosomes. The NaCl concentration was reduced by stepwise dilution and the products resolved on PA glycerol gels in order to separate mononucleosomes from free DNA. The percentages of the labeled DNA incorporated into mononucleosomes are shown.

curved molecules as well as onto the DNA template with the ATAT repeat which does not display intrinsic curvature. The relative order of inhibition was AATT > AAAA > ATAT for the three drugs, and DAPI was at least 5-fold more effective at inhibiting the assembly of each of these templates into nucleosomes as compared to distamycin or Hoechst.

The top of Figure 3 shows the frequencies and distributions of A/T sites >3 bp in length in the natural DNA fragments used as templates in nucleosome assembly reactions. Figure 3A shows that DAPI is approximately 5-fold more effective at inhibiting the assembly of a nucleosome onto the highly curved intron segment as compared to the other two MGBD. Similarly, DAPI was the most effective drug tested at inhibiting nucleosome assembly onto fragments containing a functional yeast centromere (Figure 3B), the A + T-rich domain of the yeast replicator ARS1 (Figure 3C), and a mammalian fragile site (*51*) that displays sequence and structural properties that are characteristic of origins of replication (A. H. Palin, D.J.F., C. J. Farr, and J.N.A., data not shown). These observations suggest that intrinsic DNA curvature is not needed for the drug inhibitory action since the multiple A/T tracts in these three fragments avoid a 10−11 bp periodicity (*42*, *52*, *53*). Consequently, these fragments migrate faster than expected from their lengths and base compositions on PA gels and are thus thought to be preferentially straight (*42*, *53*). The marked template specificity of DAPI and Hoechst for the A + T-rich fragments in Figure 3A−C (68−74% A + T) is clearly illustrated by the

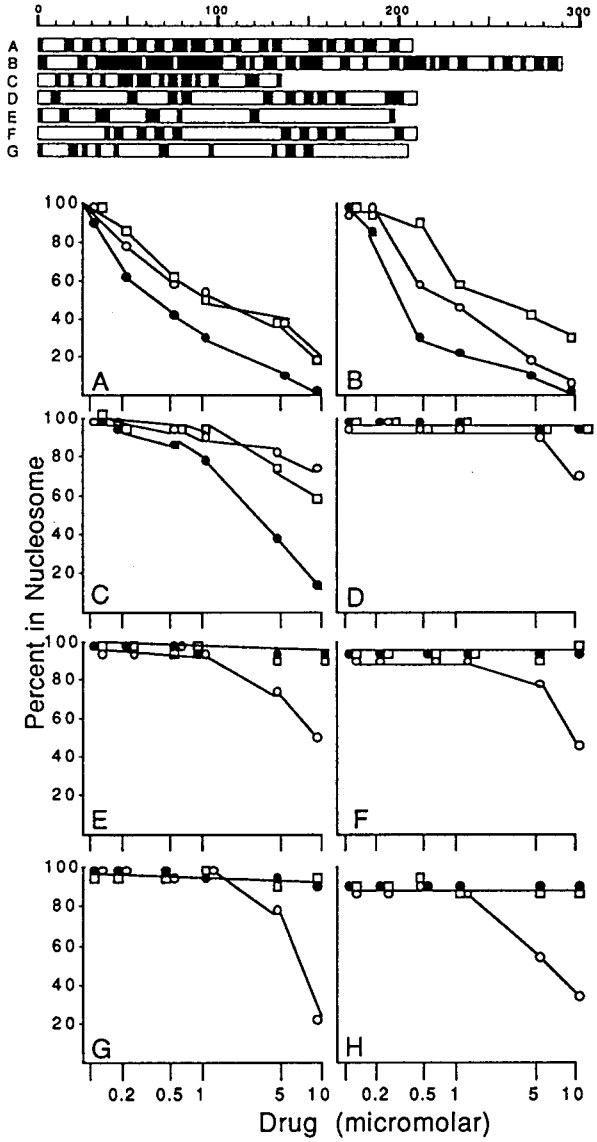

FIGURE 3: Effects of MGBD on the assembly of natural DNA into nucleosomes. The maps at the top of the figure give the distributions of A/T sequences >3 bp in length (■) in the DNA fragments used in the nucleosome reconstitutions reactions. The scale bar is in bp. The fragments are the following: (A) the intron segment from the *C. elegans* RNA polymerase gene (*46*); (B) yeast CEN III (*Bam* H1 cut) (*42*); (C) yeast ARS 1 segment containing the consensus sequence (*Nhe* I + *Pst* I cut) (*42*, *52*); (D) yeast ARS 1 segment containing the curved sequence (*Pst* I + *Hind* III cut) (*42*, *57*); (E) 5S rDNA (*Eco* R1 cut) (*47*); (F) synthetic nucleosome positioning sequence 67 (*47*); (G) exon segment from the *C. elegans* RNA polymerase gene (*46*). In the bottom panels, nucleosome reconstitutions were carried out as in Figure 2 using the indicated DNAs in the presence of the indicated concentrations of DAPI (●), distamycin (○), or Hoechst (□). Total mononucleosome DNA (145−180 bp) from wheat germ was used in panel H.

results in panels D−H which show that these ligands have no significant effects on the assembly of nucleosomes onto two moderately curved fragments (D, F), two noncurved fragments (E, G), and genomic DNA (H). The inability of these drugs to inhibit the assembly of nucleosomes onto fragments D−G can be attributed to the absence of long (>40 bp) stretches of DNA along these control templates that lack A/T sites (*41*). In contrast, the higher concentrations of distamycin (5−10 μM) inhibited the formation of nucleosomes on these control templates.

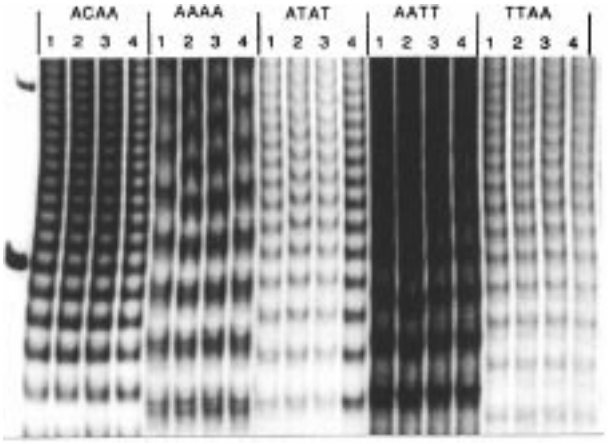

FIGURE 4: Effects of MGBD on the electrophoretic mobilities of synthetic DNAs. Synthetic duplex DNAs of the form $(CGGGN4CC)_{1-50}$ where *N* is indicated in the figure were incubated for 30 min at room temperature with no drug (lanes 1) or 10 μM DAPI, distamycin, or Hoechst (lanes 2−4, respectively) prior to electrophoresis on this 9% PA gel. The far left lane contains marker DNA with a 100 bp repeat. The figure shows only that portion of the autoradiogram that contains the 100 and 200 bp marker fragments.

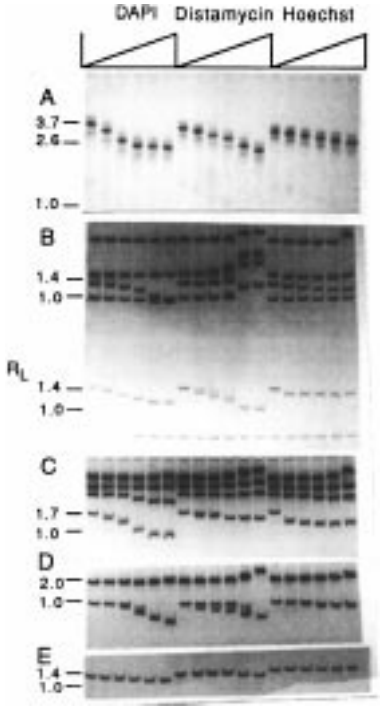

FIGURE 5: Effects of MGBD on the electrophoretic mobilities of curved natural DNAs. DNA fragments were incubated for 30 min at room temperature with the indicated drugs prior to electrophoresis on 9% PA gels. The MGBD concentrations are 0, 0.5, 1, 2, 5, and 10 μM and are indicated as the upward slanting triangle. The fragments are the following: (A) the intron segment (*46*); (B) pTRPl−ARSI−URA3 (*Eco*RI + *Hind*III + *Pst*I cut) containing two bending elements associated with ARS1 (*57*); (C) pCE (*Eco*RI + *Pvu*II cut) containing the adenovirus control region (*42*); (D) pSYN47 (*Pvu*II cut) and (E) pSYN47 (*Eco*RI + *Hind*III cut) (*47*). R_L values in the absence of drugs and the gel positions expected if the corresponding fragment had migrated according to length ($R_L = 1.0$) are indicated. The actual lengths of the indicated fragments in A−E are 192, 629, 209, 476, 400, and 129 bps.

We have previously shown that DAPI destabilized a nucleosome that had been previously assembled onto the intron segment since the drug-treated nucleosome but not the drug-free nucleosome was dissociated from the template by 0.5 M NaCl (*41*). This approach was taken in the present study to access the potencies of the three drugs for destablizing nucleosomes assembled onto the templates shown in Figure 3. The results of these experiments were similar to those shown in Figure 3 in that DAPI was the most effective of the three MGBD in destablizing nucleosomes assembled onto templates A−C but had no apparent effect on nucleosomes assembled onto templates D−H (data not shown). In addition, the inhibitory effects of higher concentrations of distamycin on the nucleosomes assembled onto the control templates D−H was also observed in these experiments.

Electrophoretic and Ligation Analysis. Previous studies have shown that the MGBD enhance the stiffness of the DNA backbone and render it resistant to thermal-induced bending (*1*, *15*). These ligands have also been reported to reduce the curvature of bent DNA (*21*, *28*, *44*, *54*−*56*; but see ref *23*). Since the DNA must bend tightly around the histone octamer in order to be assembled into a nucleosome, the inhibition of this bending by the MGBD could explain the drug-inhibitory effects seen in Figures 2 and 3 and discussed above. Thus, it was of interest to determine if the effects of the drugs on the nucleosome could be correlated with their effects on the curvature of naked DNA. Electrophoresis on PA gels is a common method used to access DNA curvature since bent fragments migrate slower than expected from their lengths. As shown in Figure 4, the synthetic duplex DNA fragments with the ACAA, ATAT, and TTAA elements migrated according to their chain lengths on PA gels in the presence and absence of the three MGBD. The relative lengths (R_L = apparent length/actual length) of these fragments ranged from 0.95 to 1.05. In contrast, the R_L values of the sequences containing the AAAA and AATT motifs that are longer than 150 bp were greater than 1.50 and these values were substantially reduced by DAPI but not by distamycin or Hoechst. Careful inspection of these and similar gels revealed that the relative drug inhibitory activities (DAPI ≫ distamycin > Hoechst) were similar to those seen in the nucleosome studies in Figure 2 for both of the synthetic curved sequences.

The enhanced activity of DAPI was also observed with a variety of natural DNA fragments as shown in Figure 5. DAPI normalized the electrophoretic mobilities of the moderately bent fragments from the yeast ARS1 (Figure 5B), the major adenovirus transcription control region (Figure 5C), and a synthetic DNA sequence (D and E) that can position a nucleosome at a single site. In addition, the drug reduced the mobility of the strongly bent intron segment at lower concentrations and to a greater extent than was seen with distamycin or Hoechst (Figure 5A). Hoechst dye was the least effective drug tested since it did not normalize the mobilities of any of the bent molecules examined in Figure 5. The relative effectiveness of distamycin was difficult to assess precisely because this drug produced a dual effect on electrophoretic mobility which has been noted previously (*54*) and which can be seen in the gels shown in Figure 5B−D. The drug reduced the gel anomaly of bent molecules but, at the same concentrations, promoted the electrophoretic retardation of otherwise nonbent sequences. The latter effect, which was most pronounced with larger fragments, presumably resulted from the formation of bent structures in nonbent DNA rather than DNA charge neutralization by the ligand

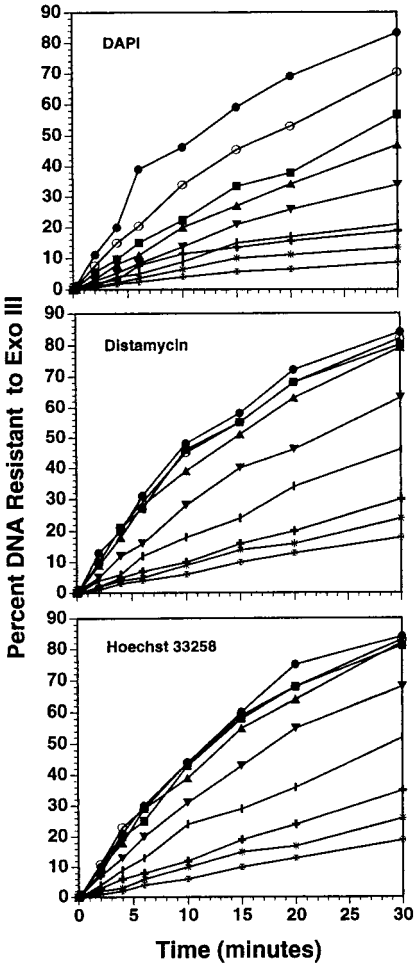

FIGURE 6: Effects of MGBD on the rate of cyclization of the intron segment in ligation reactions. The end-labeled intron segment was ligated in the presence of increasing concentrations of the indicated drugs. At the times indicated, linear DNA was degraded by ExoIII and the resistant circular forms were quantified by scintillation counting: No drug (●); 0.2 μM (○); 0.5 μM (■); 1.0 μM (▲); 2 μM (▼); 5 μM (|); 10 μM (+); 15 μM (∗); 20 μM (⌖).

since all fragments analyzed in Figure 5 migrated in agarose gels according to their chain lengths in the absence and in the presence of the MGBD (data not shown). Thus, distamycin displayed a reduced template specificity relative to DAPI and Hoechst as revealed by both electrophoretic and the nucleosome analysis. The same relative inhibitory activities as those shown in Figure 5 were seen when the drugs were incorporated into the gel and the running buffer (data not shown), suggesting that ligand dissociation during electrophoresis was not responsible for the differential drug effects.

In a previous study, we showed that the curved intron D segment preferentially formed a covalently closed circle during ligation reactions when compared to similar size nonbent fragments and bent fragments with noncircular shapes (*46*). The measurement of the cyclization of this segment in the presence of DNA binding drugs should provide a method independent of electrophoretic mobility for the assessment of the effects of ligand binding on DNA structure and anisotropic bendability. In Figure 6, the curved element was ligated in the presence of increasing concentrations of the DNA binding drugs. The fraction of the products that cyclized, as evidenced by resistance to ExoIII digestion,

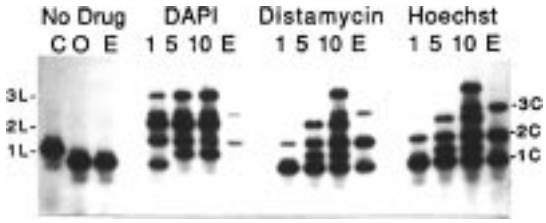

FIGURE 7: Electrophoretic analysis of ligation products. The curved intron segment was ligated for 30 min in the presence of the indicated drugs. Drug concentrations, in μM, are given above each lane. The products of the ligations were resolved on 2% agarose gels containing ethidium bromide. An ExoIII digest of the products of ligation at the highest drug concentration is also shown for each drug (E). Unligated control (C) and ligation in the absence of drug (O) are noted. Linear monomer, dimer, and trimer (1L, 2L, 3L, respectively) and circular monomer, dimer, and trimer (1C, 2C, 3C, respectively) are also marked.

was then determined at the indicated ligation times. Each drug reduced the rate of cyclization of the intron segment in a dose-dependent manner, and DAPI was 5−10-fold more effective than distamycin or Hoechst. An electrophoretic analysis of ligation products from a similar experiment is shown in Figure 7. In the absence of drug, the intron segment formed closed monomer circles which were resistant to ExoIII, as was seen in our previous study (*46*). At 1 μM DAPI, there was a decrease in the levels of monomer circles and an increase in multimer circular and linear forms. At higher concentrations of this drug, the multimeric circles disappeared which resulted in a near complete loss of DNA signal in the ExoIII-treated sample. These general trends were also seen with Hoechst and distamycin, but the concentrations required to elicit these effects were about 10-fold greater than that required with DAPI.

Drug Binding. The differential activities of the MGBD seen in Figures 2−7 could be due to differences in drug binding affinities for AT sequences, differences in AT binding specifities, or differences in the intrinsic activities of the ligand−DNA complexes. To investigate these possibilities, a series of drug−DNA binding experiments were performed. Figure 8 shows the binding of DAPI and Hoechst to synthetic DNAs as measured by fluorescence enhancement. The relative order of presumptive binding to these sequences was essentially identical for both drugs (AAAA = AATT ≫ ATAT > TTAA > AACA). This binding order is inversely related to the width of the DNA minor groove that is expected to be displayed by these sequences (*10, 50, 59*−*61*). The results in Figure 8 can explain the differential activities of DAPI since the order of DAPI binding paralleled the activities of this drug for inhibiting both the nucleosome assembly (Figure 2) and the intrinsic DNA curvature (Figure 4) of these sequences. However, the results cannot readily explain the low activity of Hoechst relative to DAPI. Similarly, the binding of DAPI and Hoechst to the curved intron segment from *C. elegans* yielded similar binding constants (K_d apparent = 2.0 and 1.5 μM for DAPI and Hoechst, respectively) yet DAPI was more effective than Hoechst in inhibiting the curvature and bendability of this fragment (Figures 3 and 5−7).

Drug footprinting experiments were conducted to further characterize the interaction of the ligands with specific oligonucleotide-length AT-rich sites. Multiple enzymatic and chemical probes were used in these studies since some probes

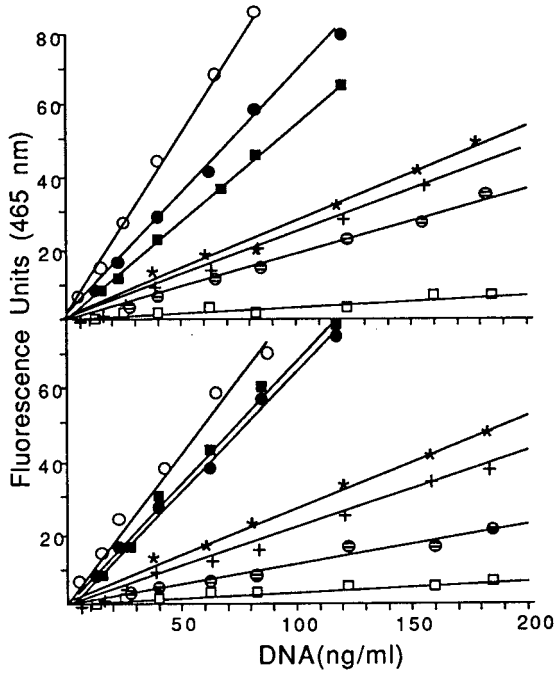

FIGURE 8: Enhancement of DAPI (top panel) and Hoechst (bottom panel) fluorescence by synthetic and natural DNAs. The fluorescence of 0.2 μM dyes at 465 nm was determined in the presence of increasing concentrations of synthetic DNAs from Figure 2 which contain the AAAA (●), AATT (■), ATAT (∗), TTAA (⊖) and AACA (□) sequence motifs. Values for the intron segment (○) and genomic DNA (+) from wheat are shown for comparison. Separate binding assays carried out under conditions of vast drug excess yielded linear Scatchard plots with the AAAA, AATT, ATAT, and TTAA DNAs, and these plots were characterized by K_d apparent values of 10, 10, 20, and 50 nM for DAPI and 10, 10, 25, and 60 nM for Hoechst.

apparently detect bound drug directly while others presumably recognized local structural perturbations in DNA induced by drug binding (*17*−*19*, *22*, *28*, *50*, *62*, *63*). The experiments were carried out with the curved intron segment as a source of natural DNA and a nucleosome positioning sequence that contains segments of synthetic curved DNA.

ExoIII was used to analyze the interaction of the drugs with specific sites in the intron sequence. To our knowledge, ExoIII has not been used previously to study noncovalent interactions of drugs with DNA. By analogy to studies of protein−DNA interactions, we assumed that the nuclease would pause directly at sites of bound drug or at sites of DNA distortion such as those that might result from ligand-induced local variations in the structure of the DNA minor groove. In Figure 9, a 322 bp DNA fragment containing the curved intron segment was incubated in the presence of the indicated concentrations of the three drugs. These concentrations spanned the range of those used in Figures 2−7. Complexes were then digested in a 3′ to 5′ direction by ExoIII and the resistant DNA analyzed on sequencing gels. Fragments containing both 5′-end-labeled upper (top gel) and lower (bottom gel) strands were subjected to the procedure so that pause sites could reliably be mapped along most of the length of the molecule. The 21 AT sites containing ≥4 nucleotides are highlighted and numbered along the sequence in the bottom of the figure with the curved element residing between the *Eco*RI sites (sites 2 and 20). The corresponding drug-induced ExoIII pauses are numbered on the vertical axes of the gels.

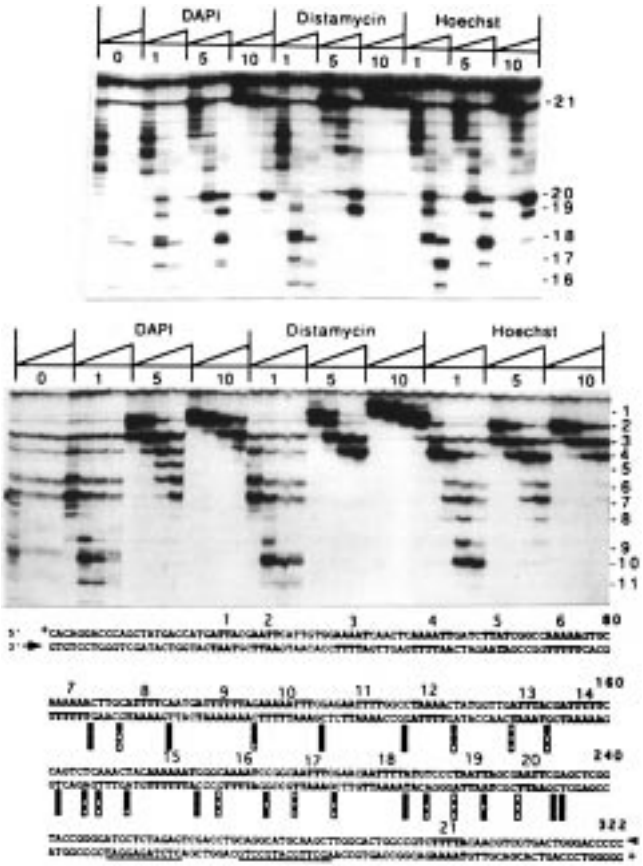

FIGURE 9: Detection of presumptive drug binding sites along the intron segment by ExoIII digestion. The 322 bp intron-containing fragment with a 5′ end-labeled top strand (top gel) and bottom strand (bottom gel) was incubated with the indicated concentrations of drugs (in μM) for 20 min prior to ExoIII (100 U/mL) addition. Samples were removed at 2, 10, 20, and 30 min (upward slanting triangle) after enzyme addition for the bottom-labeled strand and electrophoresed on denaturing gels. The 20 min time point was omitted for the top strand analysis. The sequence of the fragment is shown in the bottom of the figure. The labeled extremities (+), directions of ExoIII digestion (arrows) and all AT sites ≥4 nucleotides in length (bold face) are indicated. The gel and sequence positions of the AT sites are indicated by numbers 1−21 with the 192 bp intron segment lying between the *Eco*RI sites (AT sites 2 and 20). The two horizontal lines indicate the positions of sites rendered resistant to DNase I digestion by distamycin as determined from the data in Figure 11. Each column of three boxes below the sequence gives the DNase I sensitivity of the site to DAPI (top box), distamycin (middle box), and Hoechst (bottom box) as determined from the study in Figure 11. Filled boxes represent cutting site intensities that are unaffected or increased by the drug relative to drug-free DNA while open boxes represent site intensities that are decreased by the drug relative to drug-free DNA. The sequence positions of the ExoIII pause sites and DNase I cutting sites was assigned by reference to *Msp*I cut pUC18 markers and A and G sequencing reactions that were co-electrophoresed with the samples for varying periods of time (not shown).

The most striking result visualized on the autoradiogram in Figure 9 is that, for the most part, the three drugs induced the same ExoIII pause sites and each pause site corresponded to an AT sequence that is ≥4 bp in length. Likewise, the drugs induced ExoIII pause sites at all AT sites ≥4 bp in length in three additional fragments that were analyzed by the procedure (data not shown). The data in Figure 9 also provide general information on relative drug affinities for most sites. The three longest A−T sequences (nos. 9, 10, 18) and the two shorter homopolymeric tracts (nos. 6, 7)

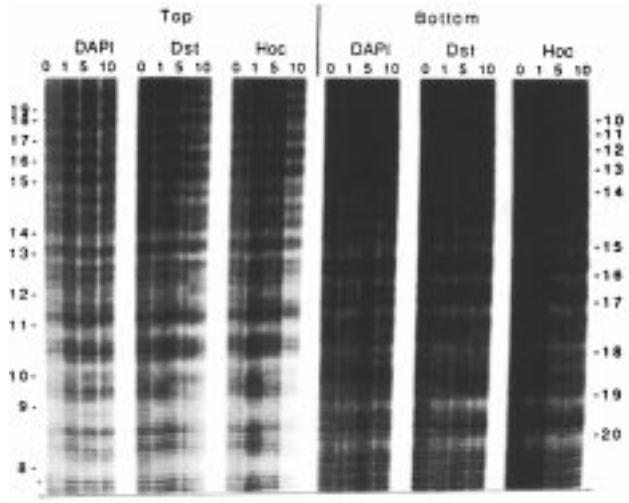

FIGURE 10: Effects of MGBD on hydroxyl radical cleavage patterns displayed by the intron segment. Intron-containing fragments with end-labeled top (left) or bottom (right) strands were incubated with the indicated concentrations of drugs as in Figure 9 prior to digestion. Abbreviations are Dst, distamycin, and Hoc, Hoechst. The gel positions of the AT sites are indicated as in Figure 9.

displayed similar drug sensitivities. ExoIII pause sites were induced in these regions by 1 μM of each ligand. In contrast, the shorter sites ($N = 4-6$ bp) composed of mixed AT sequences displayed differential drug sensitivities that can most readily be seen in the samples incubated in 1 μM drugs. The two *Eco*RI sites (nos. 2, 20) and the three additional sites with the sequence A_2T_2 (nos. 4, 17, 19) preferentially formed ExoIII pauses in 1 μM Hoechst. The relative potency of the drugs for each of these sites was Hoechst > DAPI > distamycin. Three sites with related sequences (nos. 3, 8, 16) exhibited similar drug sensitivities although the extent of induction was not as great as that seen with the A_2T_2-containing sequences. At the higher drug concentrations, pause sites appeared within the vector DNA and distamycin was clearly the most potent of the drugs in eliciting this effect. Two of these sites (nos. 1 and 21) were in AT sequences while the two additional sites centered at positions 14 and 275 were in AT-rich but mixed sequence DNA.

The results in Figure 9 provided information on the location of the regions that presumably bind with high affinity to the drugs that interact in the DNA minor groove. However, the ExoIII pause sites could not be assigned to individual nucleotides within the AT sites since high-resolution gel analysis reveal that each site was first detected as a thin band at the 3′ terminal A or T which then expanded in the 5′ direction as the enzyme progressed through the remainder of the site during the course of digestion (data not shown). Consequently, DNase I and hydroxyl radical ($OH^•$) footprinting analyses were carried out to examine the binding sites in more detail. In Figures 10 and 11, the intron fragment used in Figure 9 was incubated in the presence of the indicated concentrations of the drug prior to cleavage by these agents. For comparison, the study was also carried out with a DNA segment which contained a synthetic curved sequence of the form $[(A_5)(G/C)_5]_4$ (Figure 12). In the absence of drug, there was a preferential reduction in cutting by both DNase I and $OH^•$ at homopolymeric A-stretches and the A−T sites of the form A_N-T_N. Such reduction has been noted previously for oligo A segments in bent and nonbent

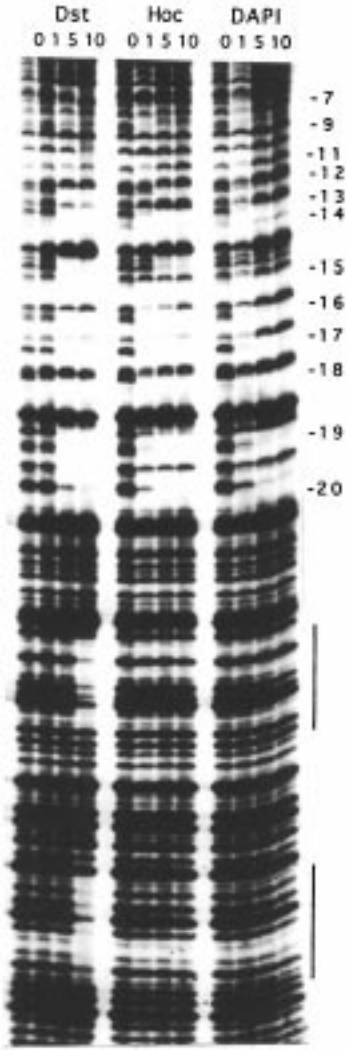

FIGURE 11: Effects of MGBD on DNase I cleavage patterns displayed by the intron segment. The 322 bp intron-containing fragment end-labeled on the bottom strand was incubated with drugs as in Figure 9 prior to digestion. The two vertical lines indicate the positions of distamycin binding sites in vector (pUC 18) DNA, and the sequences of these sites are indicated by the horizontal lines at the bottom of Figure 9. Figure 9 also gives the relative sensitivities of the DNase I sites to the three MGBD.

molecules and is thought to reflect the narrow minor groove that is characteristic of these sequences (*50*, *59*−*61*). The reduction was seen at nearly all of the A−T sites but was less pronounced in sites that contain T−A steps as seen in Figure 10 (sites 12, 18, 19). The enhanced cutting in these regions presumably resulted from T−A-dependent local widening of the DNA minor groove (*10*, *59*−*61*). In the presence of 1 μM of each of the drugs, the basic cleavage patterns persisted but the contrast was slightly enhanced principally by the further reduction in the intensities of bands at many of the A−T sites. We presume that these reductions reflect drug binding to high affinity sequences with preexisting narrow minor grooves which implies that there is little disruption of the DNA conformation upon drug binding to these sites. At this concentration, binding site sizes of 3−4 bp for DAPI and 4−6 bp for distamycin and Hoechst were estimated by $OH^•$ footprinting analysis of both bottom and top labeled strands. Increasing the concentrations of DAPI from 1 to 10 μM caused a further reduction in the band intensities of these high affinity sites, but all protected regions

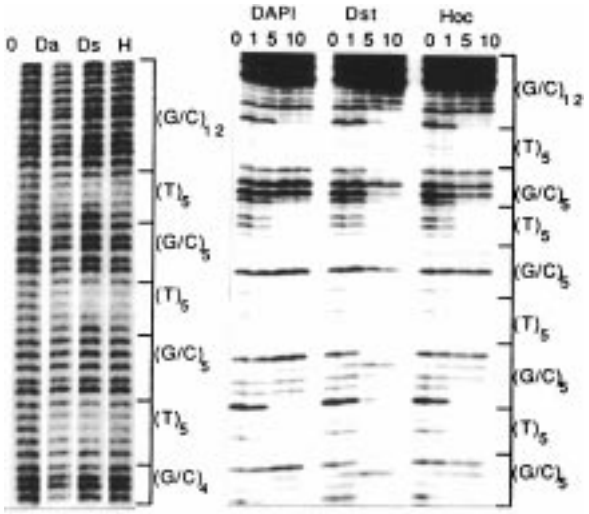

FIGURE 12: Effects of MGBD on hydroxyl radical (left gel) and DNase I (right gel) cleavage patterns displayed by the synthetic segment of a nucleosome positioning sequence. The sequence of a portion of the synthetic segment is shown. The DNase I reaction was as in Figure 11 while the hydroxyl radical cleavage reaction was performed on DNA treated with no drug (0) or 10 μM DAPI (Da), distamycin (Ds), and Hoechst (H). The hydroxyl radical lanes were cut from the same autoradiogram.

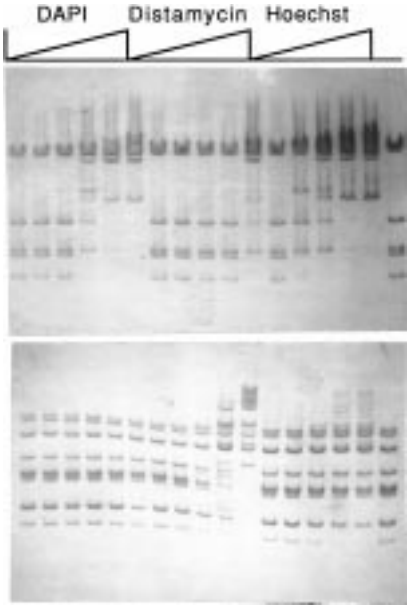

FIGURE 13: Effects of MGBD on restriction nuclease cleavage of GAATTC (top gel) and GTTAAC (bottom gel) sites in phage lambda DNA. The *Eco*R1 and *Hpa*I digestions were for 1 h at 37 °C in standard buffers using 2 U of enzyme/μg DNA. The MGBD concentrations are 1, 5, 10, 15, and 25 μM and are indicated as upward slanting triangles. Digestion products were electrophoresed on a 1% agarose gel and stained with ethidium bromide. DNA digested in the absence of drugs is shown in the far right lanes.

remained exclusively within AT sequences. In contrast, as the concentration of distamycin and Hoechst increased from 1 to 10 μM, the lengths of many of the protected regions increased to beyond the minimal binding site sizes of 4−5 bp and beyond the AT regions into flanking GC bps. This effect was particularly prevalent in the DNase I digests where distamycin and Hoechst protected between 50 and 100% of the GC bps in the sequences at 10 μM.

Essentially all of the sites protected from $OH^{\bullet}$ and DNase I cleavage by Hoechst and DAPI were centered on the same positions in the sequences, and nearly all of these positions coincided to AT sites that displayed reduced $OH^{\bullet}$ and DNase I reactivity in drug-free DNA (Figures 10−12). However, some differences were noted in the protection patterns induced by distamycin. For example, distamycin-induced low-affinity sites that were not induced by the other drugs as can be seen in Figure 11. These GC-containing sites are located between AT regions 12−13 and 17−18 and in the vector DNA, and the vector sites coincided with those seen in the Exo III digests (Figure 9). The AT region 18 in the intron segment provided an example of a drug-dependent difference in a high affinity site since 1 μM Hoechst and DAPI protected nucleotides at the 5′ end of this site which contains the 5′-A_2T_2-3′ sequence while 1 μM distamycin protected the sequence 5′-TTAT-3′ at the 3′ end. Thus, the position of the drugs within a single AT site can apparently vary in a sequence-dependent manner.

Relationship between Drug Binding and Restriction Enzyme Inhibition. Protection of AT-rich restriction sites by the MGBD provided the final assay for assessing the binding specificity of the ligands. Natural and synthetic DNAs were used in this study along with 12 enzymes with 6 bp recognition sites of variable A + T content and sequence. Examples of the analysis for two enzymes are shown in Figure 13, and the results of similar experiments for all enzymes and DNAs are summarized in Table 1. Hoechst and DAPI display similar specificities of inhibition, but cleavage was more efficiently inhibited by Hoechst than by DAPI at each site. The relative potency of the drugs for inhibiting cleavage of AT sites with narrow minor grooves (GAATTC, AAATTT) was Hoechst > DAPI ≫ distamycin (Figure 13, top; Table 1), and this order paralleled that seen in the footprinting analysis (Figures 9−11). The order of drug inhibition was different with AT sites that contained TA steps. With these sites, distamycin displayed either greater (GTTAAC) or similar (GATATC, CATATG, TTTAAA, AATAAT) inhibitory activities as compared to Hoechst and DAPI in a manner that also correlated with the footprinting studies. In addition, these sites generally required higher concentrations of drugs than the AT sites without TA steps as can be seen from the examples shown in Figure 13.

DISCUSSION

The oligopeptide distamycin A has long served as the paradigm for studies of intrinsic DNA curvature and protein-induced DNA bending. Hoechst compounds have also received considerable attention during recent years because of their effects on topoisomerase systems (*1*−*3*). However, transcription and replication depend on the assembly of multiprotein complexes onto relatively long segments of DNA and these segments often contain multiple closely spaced oligo AT sequences which may be targets for the MGBD in the cell. The results of this report clearly show that DAPI is more effective and selective than distamycin and Hoechst at inhibiting the assembly of nucleosomes onto DNA with this sequence feature. It is likely that this differential drug effect would extend to other multiprotein−DNA complexes since DAPI was more effective than the other ligands in negating the intrinsic DNA curvature and anisotropic bendability of a variety of DNA fragments including those that are involved in replication and transcrip-

tion initiation. A comparison of the results in Figures 2−7 show that the inhibitory effects of the drugs on nucleosome assembly are mirrored by their effects on the curvature and anisotropy bendability of naked DNA since DAPI was 5−10-fold more potent than the other drugs in all of the assays with each assay yielding an approximate half-maximal response in 1 μM DAPI. The most straightforward interpretation of these correlations is that the nucleosome action of the drugs is due to the inhibition of bending into narrow or compressible minor grooves of AT sequences which occurs during nucleosome formation. We considered the possibility that the differential potencies of the three drugs resulted from different affinities for the A-tract molecules, but the results in Figure 8 and studies by others (*15*, *24*, *26*, *27*) seem to argue against this view. It is also unlikely that the differential drug effects resulted from binding to different AT regions since the binding sites for Hoechst and DAPI were centered on the same positions as revealed by drug footprinting analysis and as inferred from the results of restriction nuclease protection assays (Figures 9−13 and Table 1). Likewise, the preferential action was apparently not related to the length of the AT drug binding sites since DAPI was the most effective of the MGBD at inhibiting the curvature of synthetic DNA templates containing A_4 (Figures 2 and 4) and A_5 (Figure 5) and natural DNAs with AT sites that averaged 4 bp to 7 bp in length (Figures 3 and 5−7). Different drug residence times on the binding sites are presumably not responsible for the drug-dependent variations since addition of nonradioactive intron DNA to drug-treated radioactive DNA promoted similar extents of dissociation of each of the three ligands as seen by ExoIII digestion studies (data not shown). Taken together, the results imply that the differential effects of the MGBD on the DNA conformation are not caused by differential ligand binding.

Studies on the crystal structures of the three MGBD bound to the dodecamer CGCGAATTCGCG do not seem to provide a straightforward explanation for the enhanced effects of DAPI observed in Figures 2−7. A prominent response to drug binding is the opening of the minor groove of the A_2T_2 sequence and the bending of the helix axis backward across the region of attachment (*6*−*13*). This effect could be responsible for the normalization of the electrophoretic mobility of curved DNA by the MGBD as pointed out by Burkhoff and Tillius (*50*) since the drug-induced deflections should be in the opposite direction of A-tract-induced curvature (*64*, *65*). However, the larger crescent shaped Hoechst and distamycin-like molecules deflect the backbone of the A_2T_2 sequence to a greater extent than DAPI, presumably because the shorter DAPI exerts less leverage on the helix axis (*9*). The MGBD displace the ordered spine of hydration in the minor groove (*1*, *2*, *6*, *9*, *31*), and dehydration leads to a loss of intrinsic curvature (*66*). However, DAPI might be expected to be the least effective in promoting desolvation and crystal structures of the three drug complexes seem to support this view (*9*).

An understanding of the mechanism responsible for the enhanced effects of DAPI requires a description of the mode of action of the drug footprinting reagents used in our studies. Hydroxyl radical accessibility is thought to reflect the bound drug directly (*50*, *60*, *63*), and the results presented in Figures 10 and 12 are consistent with this view. The sites protected from $OH^{\bullet}$ cleavage by all of the drugs contained principally AT bp, and the binding site sizes (4−6 bp for distamycin and Hoechst and 3−4 bp for DAPI) are similar to those derived by X-ray analysis and previous chemical protection experiments (*9*, *15*, *18*, *19*, *22*, *25*, *63*). We also suggest that the drug-induced Exo III pause sites seen in Figure 9 reflect the bound ligand since they occur at AT sites but not in the intervening DNA between these sites. In fact, Exo III appears to be a more reliable probe for drug bound to high-affinity sites than $OH^{\bullet}$ since the enzyme generated lower gel background in the drug-free DNA samples (Figures 9−12; additional data not shown). DNase I has been proposed to be a probe for structural perturbations in the minor groove of DNA (*67*), and we interpret our results according to this view. Distamycin and Hoechst promoted the protection of 2−3 GC bp that flank the AT binding sites from DNase I digestion, and this effect was particularly pronounced in the GC bp that reside between two closely spaced A tracts. Thus, these drugs impose an influence on all or nearly all GC bp in sequences of the form $[(A_5)(G/C)_5)]_N$ as seen in Figures 11 and 12. DNase I preferentially cleaves the DNA in the minor groove of medium width as compared to DNA with narrow or expanded minor grooves (*67*). The drug-induced expansion of the minor groove in GC bp that flank the AT sites could be responsible for the observed distortions induced by distamycin and Hoechst as suggested by others (*17*). The expansion of the minor groove in DNA that flanks the AT binding sites also provides a plausible mechanism that could explain the low intrinsic activities of the distamycin and Hoechst DNA complexes relative to the complex formed by DAPI. Perhaps the most effective way for a ligand to reduce global DNA curvature and anisotropic bendability into the minor groove would be to selectively antagonize each AT sequence element that is responsible for these effects. Models that associate curvature with AT sites argue that curvature results from compression of the minor groove which occurs at sequences of the form A_N or $A_N{\cdot}T_N$ (*65*). Accordingly, there should be a relationship between the selectivity of a drug for narrow minor groove sites and curvature inhibition. The most likely interpretation of the results in Figures 10−12 is that DAPI interacts very selectively with minor groove sites of minimal widths and these sites presumably correspond to those that are the centers of intrinsic curvature and bendability in drug-free DNA. Additional support for this view was provided by our previous studies which demonstrated that the DNase 1 cutting pattern displayed by the intron DNA in the nucleosome in the absence of drug was essentially identical to the cutting pattern displayed by naked intron DNA in the presence of DAPI (*41*). Consequently, each helical deflection induced by an AT site in the absence of the drug may be countered by an opposite deflection induced by DAPI binding thus effectively inhibiting nucleosome formation and global curvature. In contrast, the deflections induced by Hoechst and distamycin binding to AT sites would tend to be canceled by the deflections that arise from the expansion of the GC minor grooves because these grooves are located on the opposite face or at least on a different face of the DNA helix.

Most previous studies aimed at understanding the biological actions of the MGBD have focused on the abilities of the ligands to inhibit the binding of regulatory proteins to short AT-rich recognition sequences. DAPI has been reported to exhibit weaker activities than distamycin and/or Hoechst

in the few comparative studies that have been made (*37*, *38*, *68*). To our knowledge, the DAPI fragile sites provide the only known previous example of a MGBD action that is preferentially induced by DAPI, but the DNA targets for this effect have not been clearly defined (*69*). We attempted to model the action of the MGBD at the local sequence level by comparing ligand activities on inhibiting the cutting of restriction enzymes with AT-rich recognition sites. Previous studies have suggested that this action is related to drug binding and to local drug-induced distortion in the vicinity of the restriction sites (*1*, *36*, *40*). The results presented in Table 1 and Figure 13 demonstrated that enzyme cleavage at each site was more efficiently inhibited by Hoechst and/or distamycin than by DAPI. These results suggest that the DAPI−DNA complex is not intrinsically more active at the local sequence level than the DNA complexes formed with distamycin or Hoechst. The results also revealed that the inhibitory effects were qualitatively related to the binding specifities of the drugs as deduced from the studies in Figures 8−12. For example, both binding and inhibition of enzyme cutting in response to DAPI and Hoechst followed the general order $A_2T_2 \gg T_2A_2 >$ ATAT. The apparent affinity of Hoechst for A_2T_2 was similar to its affinity for homopolymeric A tracts, and these tracts were high-affinity binding sites for each of the drugs (Figure 9). Hoechst and DAPI also protected selectively an A_2T_2 sequence within a longer AT site in the intron segment while distamycin was apparently bound to adjacent nucleotides within the site (Figure 10). The marked preference of Hoechst for A_2T_2 had been noted previously in DNase I footprinting studies using synthetic DNA (*62*), and this drug has been shown to interact selectively with A_2T_2 in the oligonucleotide GGTAATTAC (*29*). The general sequence specificity of these drugs is inversely correlated with minor groove width (Figures 8−12) and directly correlated with sequence patterns that give rise to DNA curvature (*64*, *65*). The similarities displayed by the two drugs are reflected in crystal studies which have shown that the phenyl ring and indole ring of DAPI occupy the same positions along the dodecamer CGCGAATTCGCG as are occupied by the phenol and the first benzimidazole of Hoechst (*9*). The narrow minor groove requirement for distamycin binding appears less stringent than for Hoechst and DAPI since this drug can better tolerate GC bps and TA steps even in the center of its binding sites as revealed by ExoIII digestion studies (Figure 9) and footprinting experiments with hydroxyl radical and DNase I (*18*, *19*, *22*, *28*, *62*, *63*; Figures 10−12). The restriction nuclease studies in Figure 13 and Table 1 are also consistent with this view since the effectiveness of distamycin for inhibiting cleavage of the GTTAAA and TTTAAA sites was at least as high as for the GAATTC site. We suggest that the more indiscriminate binding of distamycin to mixed sequence DNA is responsible for the preferential reductions in electrophoretic mobilities of nonbent fragments caused by this drug and the inhibition of nucleosome assembly onto templates that lack AT clusters (Figures 3 and 5). This effect may be analogous to the bending induced at non-A-tract sequences that is produced by the covalent minor groove binder CC-1065 (*70*). The action may also be related to the 2:1 side-by-side binding mode of distamycin which is not seen with DAPI or Hoechst (*2*, *14*). A narrow minor groove is apparently not a prerequisite for distamycin binding in this mode, and the binding produces more helical distortion than a single drug molecule bound at the site (*14*).

Members of the diverse family of proteins that interact in the DNA minor groove often display highly specific biological actions. This family includes HMG chromatin architectural proteins, HMG-box transcription factors, and the TATA box binding protein (TBP). These proteins, like the drugs studied in this report, bind to AT sites with modest sequence specificity which appears to be dictated principally by structure of the DNA minor groove. A central question frequently posed about these proteins is the nature of the mechanism responsible for their biological specificities. The formation of a productive TBP−TATA box complex correlates with the structure of the complex and not with the initial binding of TBP to a TATA-like sequence (*71*). This observation seems analogous to the enhanced effect of the DNA−DAPI complex on global features of DNA described in this report and thus points to an additional similarity between minor groove binding drugs and an important class of DNA binding proteins.

ACKNOWLEDGMENT

We thank Drs. P. T. Gilham, S. Nasr, A. Stein, and I. Tessman for critical review of the manuscript and B. Atkinson for assistance in manuscript preparation.

REFERENCES

1. Zimmer, C., and Wahnert, U. (1986) *Prog. Biophys. Mol. Biol. 47*, 31−112.
2. Geierstanger, B. H., and Wemmer, D. E. (1995) *Annu. Rev. Biophys. Biomol. Struct. 24*, 463−493.
3. Turner, P. R., and Denny, W. A. (1996) *Mutat. Res. 355*, 141−169.
4. Bustin, M., and Reeves, R. (1996) in *Progress in Nucleic Acid Research and Molecular Biology* (Cohn, W. E., and Moldave, K., Eds.) pp 35−73, Academic, San Diego, CA.
5. Juo, Z. S., Chiu, T. K., Leiberman, P. M., Baikalov, I., Berk, A. J., and Dickerson, R. E. (1996) *J. Mol. Biol. 261*, 239−254.
6. Kopka, M. L., Yoon, C., Goodsell, D., Pjura, P., and Dickerson, R. E. (1985) *Proc. Natl. Acad. Sci. U.S.A. 82*, 1376−1380.
7. Teng, M., Usman, N., Frederick, C. A., and Wang, A. H.-J. (1988) *Nucleic Acids Res. 16*, 2671−2690.
8. Carrondo, M. A. A. F. de C. T., Coll, M., Aymani, J., Wang, A. H.-J., van der Marel, G. A., van Boom, J. H., and Rich, A. (1989) *Biochemistry 28*, 7849−7859.
9. Larsen, T. A., Goodsell, D. S., Cascio, D., Grzeskowiak, K., and Dickerson, R. E. (1989) *J. Biomol. Struct. Dyn. 7*, 477−491.
10. Quintana, J. R., Lipanov, A. A., and Dickerson, R. E. (1991) *Biochemistry 30*, 10294−10306.
11. Tabernero, L., Verdaguer, N., Coll, M., Fita, I., van der Marel, G. A., van Boom, J. H., Rich, A., and Aymami, J. (1993) *Biochemistry 32*, 8403−8410.
12. Vega, M. C., Garcia Saez, I., Aymami, J., Eritja, R., van der Marel, G. A., van Boom, J. H., Rich, A., and Coll, M. (1994) *Eur. J. Biochem. 222*, 721−726.
13. Tabernero, L., Bella, J., and Alemán, C. (1996) *Nucleic Acids Res. 24*, 3458−3466.
14. Chen, X., Ramakrishnan, B., and Sundaralingam (1997) *J. Mol. Biol. 267*, 1157−1170.
15. Manzini, G., Barcellona, M. L., Avitabile, M., and Quadrifoglio, F. (1983) *Nucleic Acids Res. 11*, 8861−8876.
16. Luck, G., Triebel, H., Waring, M., and Zimmer, C. (1974) *Nucleic Acids Res. 1*, 503−530.
17. Fox, K. R., and Waring, M. J. (1984) *Nucleic Acids Res. 12*, 9271−9285.

18. Schultz, P. G., and Dervan, P. B. (1984) *J. Biomol. Struct. Dyn. 1*, 1133−1147.
19. Harshman, K. D., and Dervan, P. B. (1985) *Nucleic Acids Res. 13*, 4825−4835.
20. Kubista, M., Åkerman, B., and Norden, B. (1987) *Biochemistry 26*, 4545−4553.
21. Radic, M. Z., Lundgren, K., and Hamkalo, B. A. (1987) *Cell 50*, 1101−1108.
22. Portugal, J., and Waring, M. J. (1988) *Biochim. Biophys. Acta 949*, 158−168.
23. Cons, B. M. G., and Fox, K. R. (1990) *Biochem. Biophys. Res. Commun. 171*, 1064−1070.
24. Mendoza, R., Markovits, J., Jaffrezou, J.-P., Muzard, G., and Le Pecq, J.-B. (1990) *Biochemistry 29*, 5035−5043.
25. Sarma, M. H., Gupta, G., Garcia, A. E., Umemoto, K., and Sanna, R. H. (1990) *Biochemistry 29*, 4723−4734.
26. Parkinson, J. A., Baraber, J., Douglas, K. T., Rosamond, J., and Sharples, D. (1990) *Biochemistry 29*, 10181−10190.
27. Loontiens, F. G., McLaughlin, L. W., Diekmann, S., and Clegg, R. M. (1991) *Biochemistry 30*, 182−189.
28. Radic, M. Z., Saghbini M., Elton, T. S., Reeves, R., and Hamkalo, B. A. (1992) *Chromosoma 101*, 602−608.
29. Embrey, K. J., Searle, M. S., and Craik, D. J. (1993) *Eur. J. Biochem. 211*, 437−447.
30. Eriksson, S., Kim, S. K., Kubista, M., and Nordén, B. (1993) *Biochemistry 32*, 2987−2998.
31. Chalikian, T. V., Plum, G. E., Sarvazyan, A. P., and Breslauer, K. J. (1994) *Biochemistry 33*, 8629−8640.
32. Barcellona, M. L., and Gratton, E. (1996) *Biochemistry 35*, 321−333.
33. Bruzik, J. P., Auble, D. T., and deHaseth, P. L. (1987) *Biochemistry 26*, 950−956.
34. Broggini, M., Ponti, M., Ottolenghi, S., D'Incalci, M., Mongelli, N., and Mantovani, R. (1989) *Nucleic Acids Res. 17*, 1051−1059.
35. Fesen, M., and Pommier, Y. (1989) *J. Biol. Chem. 246*, 11354−11359.
36. Dorn, A., Affolter, M., Müller, M., Gehring, W. J., and Leupin, W. (1992) *EMBO J. 11*, 279−286.
37. Chen, A. Y., C. Yu, B. Gatto, and Liu, L. F. (1993) *Proc. Natl. Acad. Sci. U.S.A. 90*, 8131−8135.
38. Chiang, S.-Y., Welch, J., Rauscher, F. J., and Berrman, T. A. (1994) *Biochemistry 35*, 321−333.
39. Welch, J. J., Rauscher, F. J., and Berrman, T. A. (1994) *J. Biol Chem. 269*, 31051−31058.
40. Forrow, S. M., Lee, M., Souhami, R. L., and Hartley, J. A. (1995) *Chem.-Biol. Interact. 96*, 125−142.
41. Fitzgerald, D. J., and Anderson, J. N. (1999) *J. Biol Chem.*, submitted for publication.
42. Anderson, J. N. (1986) *Nucleic Acids Res. 14*, 8513−8533.
43. Echols, H. (1990) *J. Biol. Chem. 265*, 697−14700.
44. VanWye, J. D., Bronson, E. C., and Anderson, J. N. (1991) *Nucleic Acids Res. 19*, 5253−5261.
45. Dobbs, D. L., Shaiu, W. L., and Benbow, R. M. (1994) *Nucleic Acids Res. 22*, 2479−2489.
46. Albert, F. G., Bronson, E. C., Fitzgerald, D. J., and Anderson, J. N. (1995) *J. Biol. Chem. 270*, 23570−23581.
47. Fitzgerald, D. J., and Anderson, J. N. (1998) *Nucleic Acids Res. 26*, 2526−2535.
48. Szabo, A. G., Krajcarski, D. T., Cavatorta, P., Masotti, L., and Barcellona, M. L. (1986) *Photochem. Photobiol. 44*, 143−150.
49. Shore, D., Langowski, J., and Baldwin, R. L. (1981) *Proc. Natl. Acad. Sci. U.S.A. 78*, 4833−4837.
50. Burkhoff, A., and Tullius, T. (1987) *Cell 48*, 935−943.
51. Palin A. H., Critcher, R., Fitzgerald, D. J., Anderson, J. N., and Farr, C. F. (1998) *J. Cell Sci. 111*, 1623−1634.
52. Eckdahl, T. T., and Anderson, J. N. (1987) *Nucleic Acids Res. 15*, 8531−8545.
53. Eckdahl, T. T., and Anderson, J. N. (1989) *Plant Mol. Biol. 12*, 507−516.
54. Wu, H.-M., and Crothers, D. (1984) *Nature (London) 308*, 509−513.
55. Griffith, J., Bleyman, M., Rauch, C. A., Kitchin, P. A., and Englund, P. T. (1986) *Cell 46*, 717−724.
56. Fitzgerald, D. J., Dryden, G. L., Bronson, E. C., Williams, J. S., and Anderson, J. N. (1994) *J. Biol. Chem. 269*, 21303−21414.
57. Williams, J. S., Eckdahl, T. T., and Anderson, J. N. (1988) *J. Mol. Cell. Biol. 8*, 2763−2769.
58. Eckdahl, T. T., and Anderson, J. N. (1988) *Nucleic Acids Res. 16*, 2346.
59. Hayes, J., Clark, D., and Wolffe, A. (1991) *Proc. Natl. Acad. Sci. U.S.A. 88*, 6829−6832.
60. Price, M., and Tullis, T. (1993) *Biochemistry 32*, 127−136.
61. Goodsell, D. S., Kaczor-Grzeskowiak, M., and Dickerson, R. E. (1994) *J. Mol. Biol. 239*, 79−96.
62. Abu-Daya, A., Brown, P. M., and Fox, K. R. (1995) *Nucleic Acids Res 17*, 3385−3392.
63. Bailly, C., and Waring, M. J. (1994) *J. Biol. Struct. Dyn. 12*, 869−898.
64. Koo, H.-S., and Crothers, D. M. (1988) *Proc. Natl. Acad. Sci. U.S.A. 85*, 1763−1767.
65. Harvey, S. C., Dlakic, M., Griffith, J., Harrington, R., Park, K., Sprous, D., and Zacharias, W. (1995) *J. Biomol. Struct. Dyn. 13*, 301−307.
66. Sprous, D., Zacharias, W., Wood, Z. A., and Harvey, S. C. (1995) *Nucleic Acids Res. 23*, 1816−1821.
67. Drew, H. R., and Travers, A. A. (1984) *Cell 37*, 491−502.
68. Straney, D. C., and Crothers, D. M. (1987) *Biochemistry 26*, 1987−1995.
69. Pelliccia, F., and Rocchi, A. (1992) *Mutat. Res. 282*, 43−48.
70. Sun, D., Lin, D. H., and Hurley, L. H. (1993) *Biochemistry 32*, 4487−4495.
71. Bernués, J., Carrera, P., and Azorin, F. (1996) *Nucleic Acids Res. 24*, 2950−2958.

BI990382P